Boron's Role in Altering MFI-type Zeolite

V. Rac[1], V. Rakić[1], A. Palčić[2], E. Dib[3], Georgeta Postole[4], Lj. Damjanović-Vasilić[5], V. Pavlović[1], S. Lević[1], S. Bosnar[2*]

[1]University of Belgrade, Faculty of Agriculture, Department of Chemistry and Biochemistry, Nemanjina 6, 11000, Belgrade, Serbia

[2]Ruđer Bošković Institute, Division of Materials Chemistry, Bijenička 54, 10000 Zagreb, Croatia

[3]Normandie Univ, ENSICAEN, UNICAEN, CNRS, Laboratorie Catalyse et Spectrochimie, 14000, Caen, France

[4]Univ Lyon, Universite Claude Bernard Lyon 1, CNRS, IRCELYON, 69626 Villeurbanne, France

[5]University of Belgrade, Faculty of Physical Chemistry, Studentski trg 12-16, 11158 Belgrade 118, P.O. Box 47, Serbia

Abstract

All-silica, boron and boron-aluminium substituted MFI-type zeolites were prepared. Different amounts of boron were added to the starting reaction mixtures to investigate their influence on the properties of the obtained zeolites. A comprehensive characterization of the materials was conducted using various techniques: X-ray Diffraction (XRD), nitrogen physisorption, Scanning Electron Microscopy (SEM), infrared (IR), Nuclear Magnetic Resonance (NMR) spectroscopy, thermogravimetric analysis (TGA) as well as microcalorimetry accompanied by ammonia adsorption. The MFI topology and crystallinity is conserved regardless the amount of heteroatoms that occupied different local environments, while the morphology of the crystals, their thermal stability, and their acidity differ considerably. For instance, boron assuming both tetrahedral and trigonal coordination, affect the interactions of the framework with both the organic structure directing agents (OSDA) and ammonia species giving rise to detectable differences in acidity.

Keywords: boron incorporation, MFI zeolite, structure, acidity

Introduction

Partial isomorphous substitution of silicon with tri- and tetravalent atoms in zeolite framework tetrahedral positions (T-atoms) is an effective method for modification of zeolites' properties and their performance as catalysts [1]. Properties of obtained zeolites are closely related to the nature, amount and location of the incorporated atoms. While Al^{3+} is the main substituent of Si^{4+} in tetrahedral positions within the zeolites' frameworks offering an acidic character to zeolite-based catalysts due to the protons equilibrating the negative charges, B^{3+} is usually used when a milder acidity is needed for specific catalytic applications [1, 2]. Thus, the substitution of Si with B was achieved in different zeolite frameworks, e.g. B-ZSM-5 [3, 4], B-BEA [4], B-SSZ-13 [4, 5]. The strength of the acid site, i.e. easiness of the detaching of proton is intimately related to the strength of the interaction between trivalent framework atoms and neighbouring oxygen atoms connected to the acidic hydroxyl group known as Brønsted acid sites [4, 6, 7]. Thus, zeolites incorporating boron usually have lower acidity compared to their gallium or aluminium counterparts, in order B < Ga < Al [1, 6, 8, 9]. Boron substituted zeolites are therefore used in the reactions demanding lower acidity as, for example the oxidative dehydrogenation of alkanes to olefine [10-12] and the methanol to olefin conversion [13, 14].

The geometrical configuration of boron in zeolites' frameworks may be trigonal or tetrahedral depending on (i) the hydration degree and the stability of B^{3+} in tetrahedral configuration, (ii) the availability of compensating cations like sodium, lithium or ammonium in the vicinity of boron [15], and (iii) the calcination procedure applied[16]. The presence of Na^+ stabilizes the tetracoordinated configuration of boron due to favourable electrostatic interactions leading to the formation of $Na^+\cdots B(OSi)^{4-}$ adduct [5, 16, 17]. However, it was found that for successful incorporation of tetrahedrally coordinated boron in the MFI structure from alkaline reaction mixture containing TPA^+ and Na^+, the presence of TPA^+ is mandatory, due to the geometrical specificity between TPA^+ and MFI topology as well as to the specific boron building units formed in the presence of TPA^+ which can be then successfully involved in the condensation processes. This is not observed when solely Na^+ cations are present in the reaction mixture [18, 19], yet the presence of Na^+ favours the condensation processes. Moreover, it was shown that TPA^+/Na^+ ratio in the synthesis mixture dictates the relative populations of tetrahedral and trigonal boron sites in the zeolite framework [15].

On the other hand, the removal of the organic cation from the zeolite structure by calcination in air leaves protonated zeolite promoting the disconnection of tetracoordinated

boron atoms into trigonal framework-associated and/or the complete leaching into extra framework boron species [15, 17, 20, 21]. Upon calcination, the protonic form of boron zeolites is very sensitive to the presence of water, the hydrolysis of B-OSi bonds happens even when zeolites are exposed to humidity at room temperature. The hydrolysis gives rise to a variety of boronous species that may keep a partial connection with two or three oxygen bridges in the framework depending on the degree of hydrolysis and the partial humidity [12, 17]. Process finishes by boron leaving the framework as trigonal $B(OH)_3$ extra framework species [17, 22].

Therefore, to remove boron from zeolite framework rather moderate post-synthesis treatments could be applied, slurry of water or mildly acidic solutions, which is less harsh than conditions usually applied for dealumination [23]. Deboronation process consists of displacing tetrahedral boron atoms from the lattice positions and induces the generation of silanol defects known as hydroxyl nests in the zeolite framework [16]. In contrast to the defects present in as synthesized silicalite-1 that arise from the charge compensation process [24], which may condense upon calcination, the defects formed by deboronation of the calcined boron containing materials are stable and they may be used to tune the catalytic activity, hydrophilicity, and functionalization of zeolites [16, 25, 26]. Namely, hydroxyl nests formed by deboronation could be repopulated by other metal cations that are not possible to incorporate into the zeolite framework, or at least not at defined positions within zeolite framework, under hydrothermal conditions in basic medium, which therefore provides opportunities to tune the acidity and optimize zeolite catalytic performance [7, 27, 28]. From previous works reported in the literature, it can be concluded that boron substituted zeolites are materials that, apart from their acidic properties, are suitable to the incorporation of heteroatoms in zeolites, serving as transitional forms for obtaining zeolites with pre-designed properties.

Based on previously mentioned tremendous properties, boron substituted zeolites represent important and promising materials for comprehensive investigation. Therefore, in this work, we have explored in detail the influence of boron incorporation on the structural properties of MFI zeolites.

Experimental

Four syntheses mixtures with a molar composition 60 SiO_2 : X B_2O_3 : Y Al_2O_3 : 2.5 Na_2O : 8 TPABr : 800 H_2O, were prepared using fumed silica (SiO_2, 99.8%, Sigma Aldrich), boric acid (H_3BO_3, 99.8%, Sigma Aldrich), aluminium hydroxide ($Al(OH)_3$, pure, Kemika), sodium hydroxide (NaOH, 98%, Kemika), tetrapropylammonium bromide (TPABr, 98%, Sigma Aldrich), and deionized water. Different scenarios were explored varying X and Y values for the 4 samples denominated accordingly as follows: S-B0Al0 (X = 0, Y = 0) ; S-B1Al0 (X = 1, Y = 0) ; S-B2Al0 (X = 2 , Y = 0) ; S-B2Al2 (X = 2 , Y = 2).

Typically, appropriate amounts of NaOH and TPABr were first dissolved in water. Then, when needed, boric acid and aluminium hydroxide were added to the solution before adding fumed silica. The gels obtained were transferred into Teflon-lined metallic autoclaves and heated in oven at 150 °C for 5 days. The obtained solids were separated, washed with water, dried at 80 °C overnight and calcined at 550 °C for 5 hours. The samples were characterized by X-ray diffraction (XRD), Scanning Electron Microscopy (SEM), Nuclear Magnetic Resonance (NMR), Fourier transform Infrared (FTIR), N_2 sorption, thermogravimetric analyses (TGA) and microcalorimetry/volumetry of ammonia adsorption as described below.

For X-ray diffraction measurements Rigaku Ultima IV diffractometer in Bragg-Braentano geometry, with Ni filtered CuK_α radiation (λ=1.54178 Å) was used. Diffraction data were acquired over the scattering angle range 2θ from 2° to 70° with a step of 0.02° and acquisition rate of 1°/min.

The morphology of the samples was investigated by scanning electron microscope JEOL JSM-6390LV. Prior to the SEM observations, the powders were coated with gold to minimize charging.

^{11}B and ^{27}Al NMR spectra were acquired at 160.4 and 130.3 MHz on a Bruker Avance III-HD 500 (11.7 T) using a Magic Angle Spinning (MAS) 4.0-mm outer diameter probehead rotating at 12 kHz. Single pulse experiments were used setting the nutation frequencies at 74 and 60 kHz respectively. $\pi/4$ and $\pi/6$ pulses were used to ensure a quantitative acquisition regardless the environment of the nuclei. Recycle delays of 2 seconds and 1 second were used respectively acquiring 256 and 148 scans. The chemical shift references used were set using saturated aqueous solutions of H_3BO_3 (20 ppm) and $Al(NO_3)_3$ (0 ppm).

FTIR spectra were collected using IRAffinity-1 (SHIMADZU) spectrophotometer; 2 mg of sample was pelletized in 200 mg of KBr (Fisher Scientific); for each spectrum 100 scans were collected with 4 cm^{-1} resolution.

Low temperature nitrogen adsorption/desorption experiments were conducted using a Belsorp Mini X apparatus. Prior to adsorption, the samples were evacuated in situ at 400 ºC for 4 h. Specific surfaces were calculated using BET method, according to the Rouquerol correction [29] for microporous materials, ISO 9277. Microporous and mesoporous surfaces and volumes were determined using t-plot method.

Thermal analyser STA 6000 (PerkinElmer, Inc.) was deployed for performing thermogravimetric analysis of the powder samples. Solids were charged in alumina crucibles and heated at rate of 5 °C min^{-1} from room temperature to 800 °C purging at a flow of oxygen gas of 30 mL min^{-1}.

Acidity was determined using microcalorimetry of ammonia adsorption. Adsorption heats were measured in a heat-flow microcalorimeter of the Tian-Calvet type (C80 Setaram), linked to a calibrated glass volumetric line. Experiments consisted of admitting small doses of NH_3 to the sample. Evolved heats and amounts of adsorbed gas were simultaneously determined per each dose, at 150 °C. Samples were pre-treated in vacuum, overnight, at 400 °C.

Results and discussion

XRD analysis

Figure 1 presents the diffraction patterns of the four calcined samples. They correspond to crystalline MFI-type zeolites without any amorphous species [14, 30, 31]. The Pn21a space group of calcined heteroatom-containing MFI-type zeolites is usually giving rise to a splitting of the peak 24° 2θ [26, 32-36]. Such splitting may be an indication of heteroatom incorporation in the zeolite framework [7, 34, 36]. Therefore, the splitting of diffraction peaks at about 24.4° 2θ in diffractograms for samples S-B1Al0, S-B2Al0 and S-B2Al2 (Figure 1 and enlarged in Figure 2), indicate a successful incorporation of boron (samples S-B1Al0 and S-B2Al0) and boron and aluminium (sample S-B2Al2) into silicalite framework.

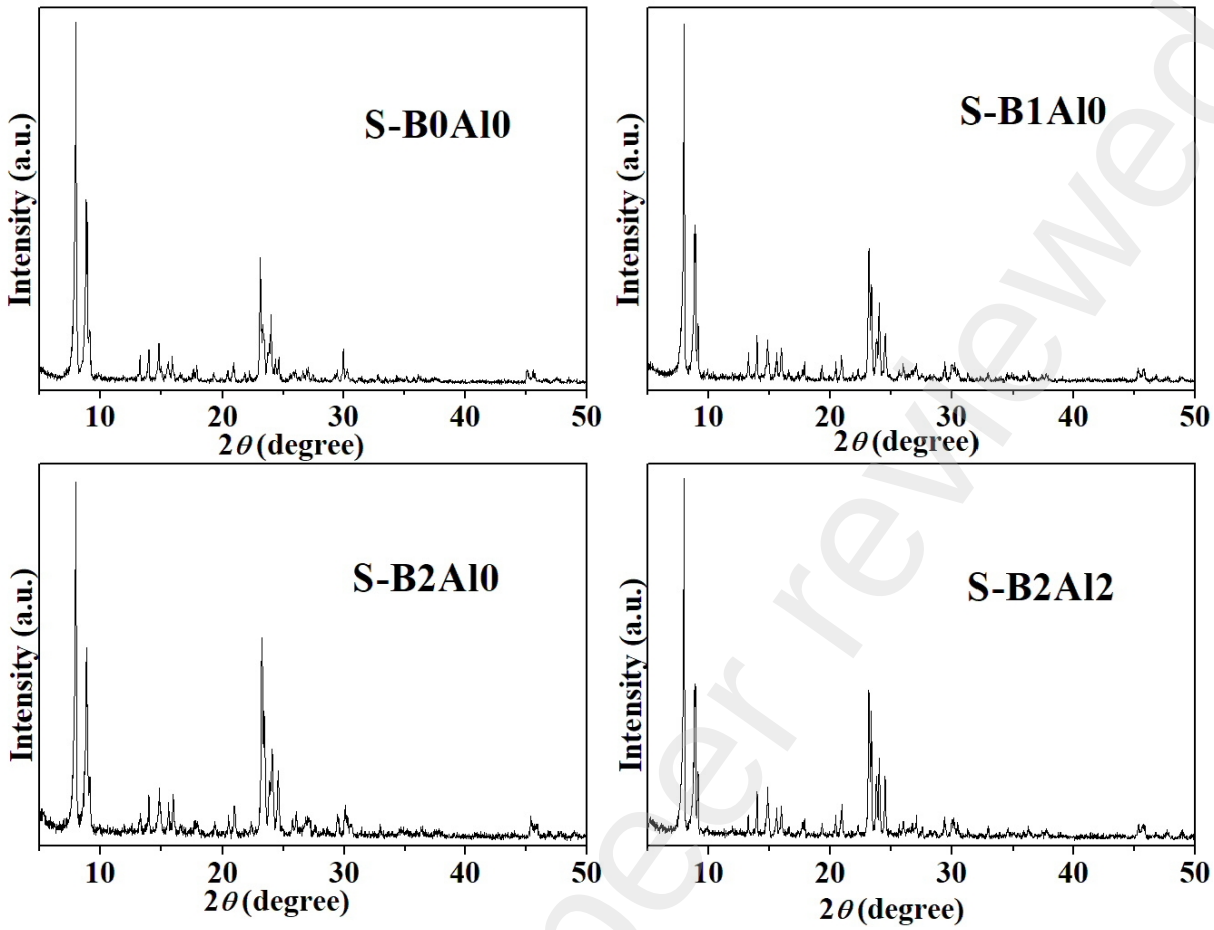

Figure 1. X-ray patterns of samples: a) S-B0Al0, b) S-B1Al0, c) S-B2Al0 and d) S-B2Al2

In Figure 2, a shift of peak positions to higher 2θ values is also noticed, and connected to the decrease of d-values, which thus points to the zeolite unit-cell contraction identified for samples S-B1Al0, S-B2Al0 and S-B2Al2 [36]. This decrease exhibits another evidence of boron's presence in the zeolite framework and arises due to smaller size of boron atom and shorter B-O bond length (1.46 Å) as compared to Si-O (1.61 Å) and Al-O bonds (1.67 Å), as well as consequent decrease of Si-O-B bond angles [36-38].

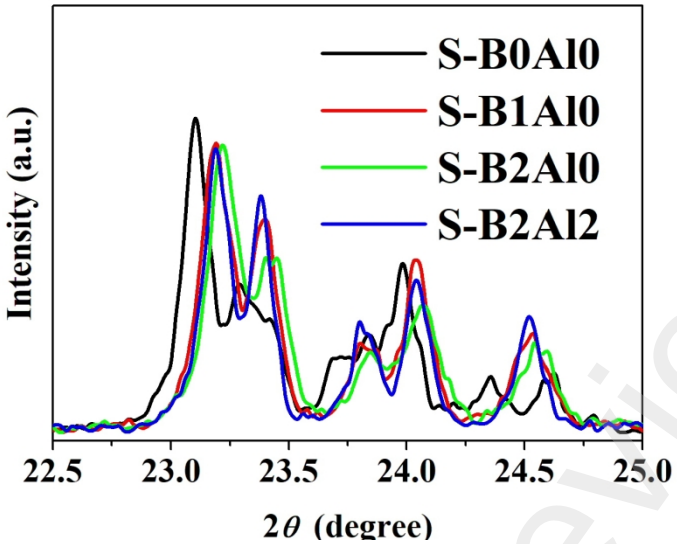

Figure 2. Enlarged part of XRD diffractograms of the studied series of samples shown in the Figure 1 in the region from 22.5 to 25° 2θ

N_2 physisorption

Nitrogen physisorption isotherms (Figure 3, Table 1) of all samples exhibit profiles typical for MFI-type materials with rather similar value of micropore volume (ca. 0.15 cm^3/g) in line with their high crystallinity degree [39, 40]. Nevertheless, the curves of each respective sample differ in character from nearly type Ib isotherm of the sample S-B2Al2 via type IVa isotherm of S-B2Al0 and S-B1Al0 to a two-hysteresis type IVa curve of the all-silica material. Type IVa isotherms of S-B2Al0 and S-B1Al0 with type H5 hysteresis loops indicates assemblies of pores having both open and partially blocked mesopores. Type Ib isotherm of S-B2Al2 suggests that the material possesses wider micropores and possibly narrow mesopores (< ~ 2.5 nm) [41]. The two H4 hysteresis loops of S-B0Al0 arise due to the capillary condensation in pores of different sizes as the inflection point positions are related to the dimensions of the pores, lower the p/p^0 value, smaller the pore diameter. Such loops are typical with aggregated crystals of zeolites.

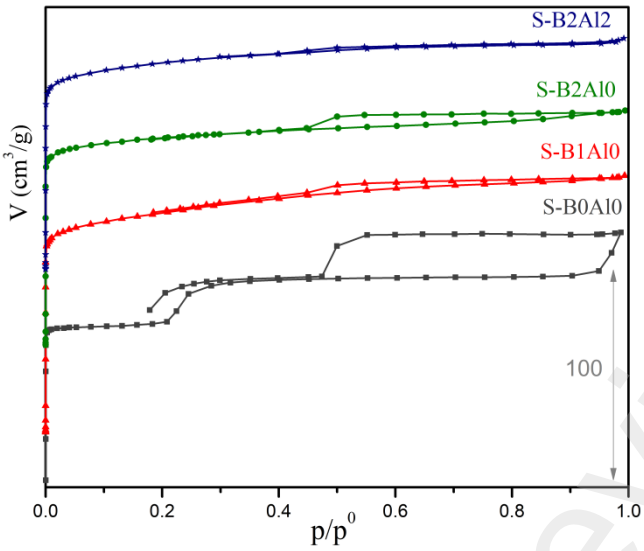

Figure 3. Nitrogen physisorption isotherms of the studied series of samples

Table 1. Textural parameters of the studied series of samples

	S_{BET} (m^2/g)[a]	S_{ext} (m^2/g)[b]	V_{micro} (cm^3/g)[b]	V_{tot} (cm^3/g)[c]
S-B0Al0	372	18	0.159	0.205
S-B1Al0	406	27	0.158	0.190
S-B2Al0	391	19	0.148	0.173
S-B2Al2	383	20	0.149	0.171

[a]BET surface, [b]from t-plot, [c] at p/p^0=0.99

SEM analysis

The particle morphologies of the samples are shown on SEM micrographs in Figure 4. The particles of the sample S-B0Al0 (Figure 4a), obtained from the parent reaction mixture, i.e. boron- and aluminium-free, have characteristic MFI-type intergrown morphology with crystal size of about 6 μm. With the addition of boron into the reaction mixture for the sample S-B1Al0 (Si/B=30, Figure 4b), the particles become more rounded, but the crystal sizes remain quite similar to the sample S-B0Al0. With further increase of the boron amount in the reaction mixture (Si/B=15, sample S-B2Al0, Figure 4c), particles become large spherical polycrystalline aggregates with size of about 17 μm, composed of many intergrown domains.

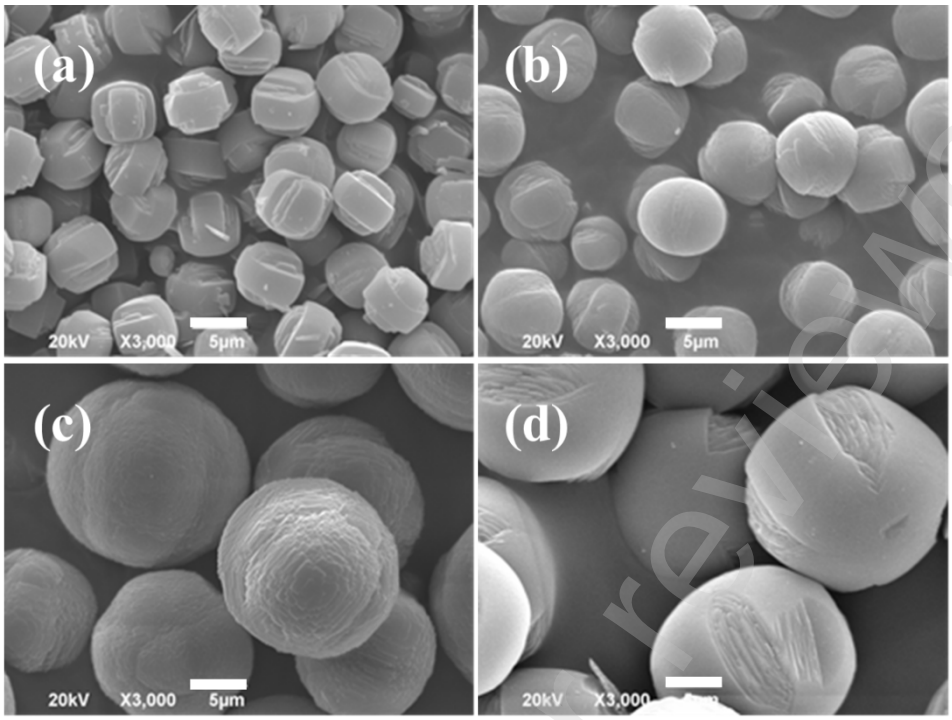

Figure 4. SEM of samples: a) S-B0Al0, b) S-B1Al0, c) S-B2Al0, d) S-B2Al2. In all micrographs bar is 5 μm.

When both aluminium and boron were present in the reaction mixture (Si/B=15, Si/Al=15), the obtained spherical crystals of the sample S-B2Al2 (Figure 4d) have size of about 16 μm, with combined smooth and polycrystalline surface domains. In addition, Figure 4 shows that by simple change of Si/B ratio in the reaction mixture it becomes possible to influence the size and shape of the obtained zeolite particles, which is in agreement with literature data [7, 42].

NMR analysis

Figure 5 shows ^{11}B NMR spectra representing the local structure of boron atoms in samples S-B1Al0, S-B2Al0 and S-B2Al2. The spectrum of the sample S-B1Al0 (Si/B=30) shows two overlapped narrow peaks at -2.2 and -0.7 ppm. On the other hand, the sample S-B2Al0 (Si/B=15, Figure 5b) exhibits a broad line around 18 ppm besides a narrow peak of high intensity at -2 ppm. A peak at 2 ppm is also observed in S-B2Al2 (Si/B=15, Si/Al=15) but with lower intensity compared to the samples S-B1Al0 and S-B2Al0. In addition, for the sample S-B2Al2, the ^{27}Al NMR spectrum shows broad bands at ~60, and ~0 ppm corresponding to tetrahedrally coordinated and extra framework aluminium species, respectively [22].

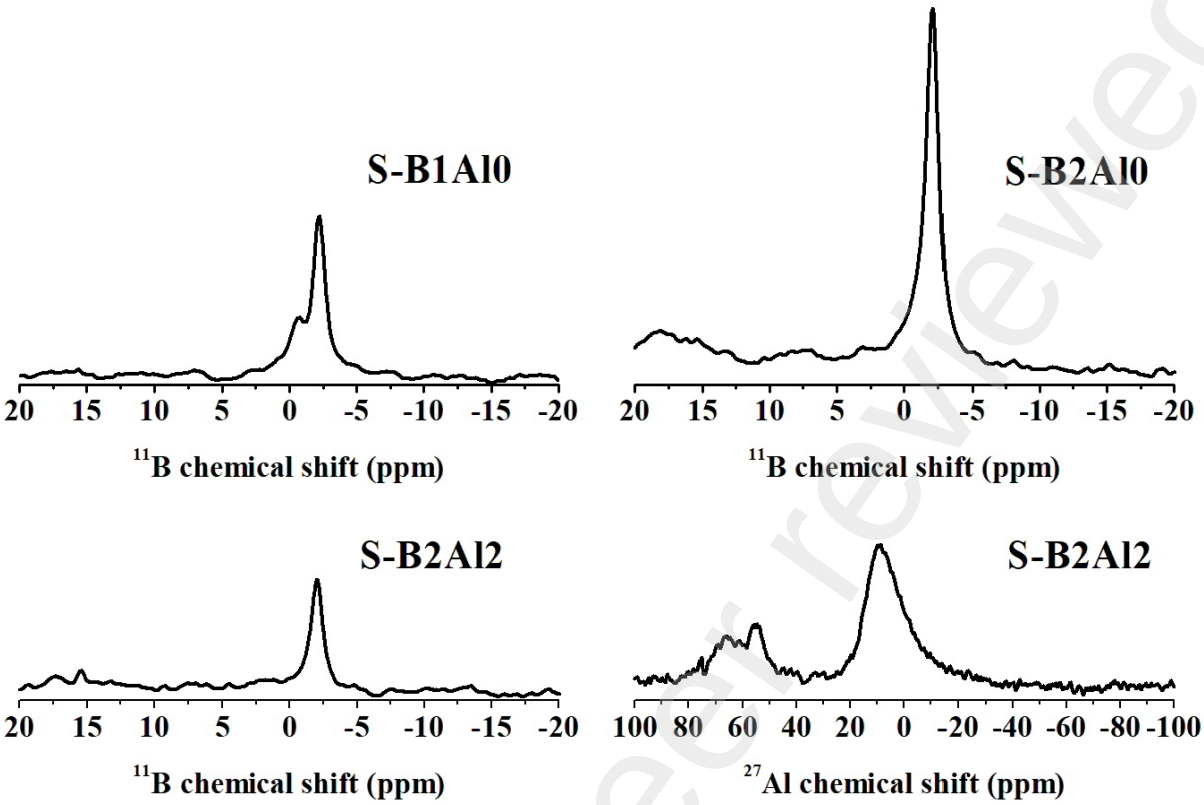

Figure 5. ^{11}B NMR spectra for samples: a) S-B1Al0, b) S-B2Al0, c) S-B2Al2; and ^{27}Al NMR spectrum for sample d) S-B2Al2

Narrow peaks of tetrahedrally coordinated framework boron in zeolites are usually observed between -1.3 to -6 ppm [16, 21, 38, 43]. Framework associated boron species containing one or more -OH bonds are observed in the same region, also being tetrahedral [5, 12, 22, 44]. The two peaks found in the sample S-B1Al0 could be interpreted as two tetrahedral environments of boron in the MFI framework composed of 24 non-equivalent tetrahedral sites when adopting the Pn21a symmetry [22]. Extra-framework trigonal boron units, BO_3, exhibit broad lines at around 20 ppm [12, 22, 43, 44], thus, the peak observed at 18 ppm in the sample S-B2Al0 is assigned to extra-framework trigonal boron species as $B(OH)_3$ [5, 12, 22, 45].

As already mentioned, upon the calcination in oxidizing environment, a part of framework boron could be transformed into trigonal and/or extra-framework boron species [20]. In addition, the proportion of trigonal and tetrahedral boron also depends on the hydration status of the sample. However, the stability of framework boron in both cases is influenced by the presence of Na^+ [5, 21, 38, 43]. Therefore, the presence of tetrahedral and

trigonal boron signals in NMR spectra of samples S-B2Al0 and S-B2Al2 can be connected to the presence of Na^+ in the starting reaction mixture.

FTIR analysis

IR spectra of all samples are shown in Figure 6. Basic vibrations of the TO_4 tetrahedra in the region from 1400 cm^{-1} to 450 cm^{-1} reflect zeolite framework structure [46]. These vibrations can originate from internal tetrahedron vibrations as well as from the external connections between tetrahedra.

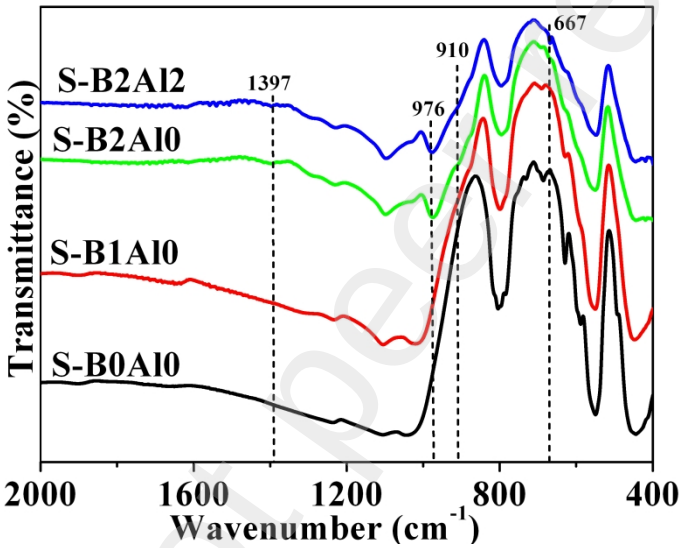

Figure 6. FT-IR spectra of the samples S-B0Al0, S-B1Al0, S-B2Al0 and S-B2Al2

All characteristic vibrations for MFI-type zeolite structure can be clearly distinguished in all samples. The band at 450 cm^{-1} can be connected to the internal T-O bending. The peak at 550 cm^{-1} can be ascribed to double 5 ring vibration (pentasyl units) and is usually taken as fingerprint of the fully crystalline MFI structure [47]. Furthermore, bands in the region from 550 to 650 cm^{-1} could be ascribed to the vibration of double rings in the zeolite framework [48, 49], more precisely for the MFI structure, to the vibration of pentasyl units with different number of (five membered rings) components [47, 50]. The band at 790 cm^{-1} can be ascribed to the symmetric T-O stretching vibration. Further, a broad peak at 1000-1300 cm^{-1} is connected to the asymmetric T-O-T stretching [51]. This broad peak consists of band at about 1220 cm^{-1}, which is also characteristic for zeolites with pentasyl framework units [48], and doublet at about 1030 cm^{-1} and 1100 cm^{-1} [52]. The doublet is more pronounced in samples S-

B0Al0 and S-B1Al0 and diminishes in the samples S-B2Al0 and S-B2Al2, which can be connected to the change in sizes of crystals [52].

The presence of boron in the zeolite structure is usually indicated by framework vibrational modes in the range 1400-700 cm^{-1} [43, 53]. A very weak band at 1390 cm^{-1} can be observed for the samples S-B2Al0 and S-B2Al2, ascribed to the asymmetric stretching vibration of B-O of the $[B(OSi)_3]$ unit [53]. Furthermore, in the spectrum region from 850 to about 940 cm^{-1} (Figure 6), a very weak and broad shoulder can be detected for the samples S-B1Al0, S-B2Al0 and S-B2Al2, which could be connected to the hydroxylated $[BO_3OH]^-$ or $[BO_2(OH)_2]^-$ units adjacent to SiO_4 tetrahedron [53]. In addition, there is a very pronounced peak for samples S-B2Al0 and S-B2Al2 at about 970 cm^{-1}. This peak is ascribed to the perturbation of SiO_4 tetrahedra which can be induced by isomorphous heteroatom insertion into framework, by the presence of neighbouring Si vacancies or by the strong interaction of extra framework cations and framework [26, 51, 54]

In borosilicate glasses, vibrations in this range are connected to the stretching vibrations of structural groups, which contain BO_4 units [55]. Taking in account very low intensity of 1390 cm^{-1} peak in samples S-B2Al0 and S-B2Al2, and NMR spectra for those two samples showing tetracoordinated boron signals it could be presumed that diminishing of the band at 1390 cm^{-1} occurs due to the interaction of boron with water, which consequently causes transformation of trigonal into tetracoordinated boron units [56]. Such an interaction demands presence of silanols in adjacent position, which have stretching vibrations at about 960 cm^{-1} [1, 43, 56]. In addition, the presence of sodium cations in boron vicinity stabilising its tetrahedral coordination could contribute to this strong peak as well [51].

Very weak bands at 670 cm^{-1} in samples S-B2Al0 and S-B2Al2 can be ascribed to the symmetric bending vibrations of Si-O-B bond [14, 31]. The absence of the weak shoulder at about 1390 cm^{-1} and the presence of strong peaks at about 970 cm^{-1} and 670 cm^{-1} as well as weak broad shoulders at 850 and 940 cm^{-1} in the IR spectrum of the sample S-B1Al0, indicate the tetracoordinated environment of boron atoms present near SiO_4 tetrahedra [53, 57]. This is in accordance with the tetracoordinated boron signal observed in the NMR spectrum (Figure 5a).

TGA analysis

Thermal properties of investigated samples are shown in the Figure 7. TG curve for the sample S-B0Al0 (Figure 7, black line) shows pronounced weight loss in the temperature

interval from 360 to 450 °C, connected to the TPA^+ degradation. Two DTG peaks (Figure 7 inset), a strong sharp peak at 397 °C and a broad peak with maximum at about 440 °C, could be ascribed to the different stages of the decomposition and elimination of TPA^+ [58, 59] bonded to the crystal defects in that sample [59-62]. The weight loss ascribed to TPA^+ removal for S-B0Al0 is 11.5%.

Thermal properties of samples S-B1Al0, S-B2Al0 and S-B2Al2 with incorporated boron/boron and aluminium atoms in the zeolite structure show different characteristics as compared to the parent S-B0Al0 sample. For samples S-B1Al0 and S-B2Al0 the TG/DTG curves show relatively slow weight loss up to 360 °C, i.e. broad and weak shoulder in the temperature interval from about 150 to 360 °C (Figure 7, red and green lines, respectively). This weight loss could be partially ascribed to the dehydration due to presence of hydrated Na^+ cations [61, 63] but mostly to the degradation of TPA^+ [58].

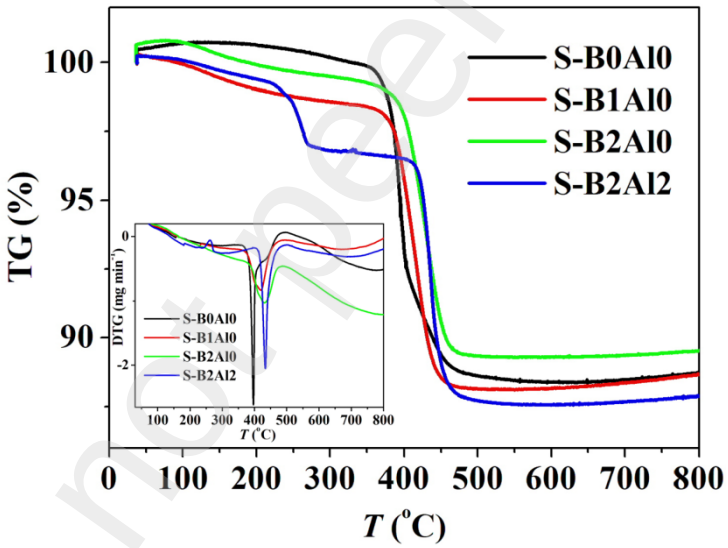

Figure 7. TG and DTG (inset) results for samples S-B0Al0, S-B1Al0, S-B2Al0 and S-B2Al2

Further pronounced weight loss from 360 to 450 °C is ascribed to further removal of confined TPA^+. The DTG curves maxima are at about 420 °C for the sample S-B1Al0 and 430 °C for the sample S-B2Al0, while the profile suggests that the degradation and elimination of framework TPA^+ proceeds slower compared to the samples S-B0Al0 (Figure 7, inset, black line) and S-B2Al2 (Figure 7, inset, blue line). The weight loss ascribed to TPA^+ removal for the sample S-B1Al0 is 10.22%, while for the sample S-B2Al0 is 9.95%.

The TG curve for the sample S-B2Al2 (Figure 7, blue line) has specific shape different from other samples, characterized by marked weight loss step at about 200 °C. In this sample both boron and aluminium atoms are incorporated in the zeolite framework, which likely

reflects in noticed specific thermal effect at about 200 °C due to their properties. Further weight loss connected to the TPA^+ removal from the framework starts at about 400 °C. DTG curve (Figure 7, inset, blue line) shows strong and sharp peak with maximum at about 433 °C. The weight loss in S-B2Al2 due to the TPA^+ removal is 8.88%.

Endothermic peaks maxima are observed for the samples S-B1Al0, S-B2Al0 and S-B2Al2 (Figure 7, inset) at 420 °C, 430 °C and 433 °C, respectively. They are shifted to higher temperatures compared to the sample S-B0Al0 for which, the maxima is observed at 400 °C. While in the sample S-B0Al0, the TPA^+ cation charge is balanced by the siloxy groups, in the samples S-B1Al0, S-B2Al0 and S-B2Al2 the negative compensating charge is brought by trivalent atoms present in the framework [58, 60]. Due to the fiercer interaction with trivalent T-atoms, TPA^+ is strongly interacting with the framework, which consequently shifts the TPA^+ degradation to higher temperature [37, 60].

In addition, the features of DTG curves for the samples S-B1Al0, S-B2Al0 and S-B2Al2 indicate that the degradation of the TPA^+ proceeds slower and over longer temperature interval for the samples S-B1Al0 (Figure 7 inset, red line) and S-B2Al0 (Figure 7 inset, green line). The degradation is accelerated in sample S-B2Al2, suggested by strong and sharp DTG peak (Figure 7 inset, blue line), which could be connected to the nature and the amount of the incorporated T-atoms influencing TPA^+-zeolite interaction.

Acidity

The acidic properties of the samples were evaluated in terms of amount and strength of acid sites. Using coupled microcalorimetry and volumetry of ammonia adsorption, calorimetric curves i.e. profiles of differential heats vs. uptake, were recorded, Figure 8. As expected, the sample S-B0Al0 (silicalite) exhibited negligible acidity, a very small amount of acid sites, all of them being very weak, with strengths below 30 kJ/mol. Upon boron introduction (samples S-B1Al0 and S-B2Al0), a pronounced increase in acidity was detected, characterized by much larger amounts of acid sites and a significant increase of the sites' strengths. Although boron content is higher in S-B2Al0, the difference in acidity is small, especially in the domain of strong sites, where the two calorimetric curves are almost identical. The addition of Al to the synthesis mixture resulted in a more puzzling effect. While the idea behind simultaneous incorporation of B and Al was to evaluate the possibility of controlling the amount and strength of acid sites, adding Al resulted in reduced acidity. It

seems that boron has a significant impact on the mechanism of Al incorporation and formation of Al-related acid sites. In the presence of boron, the addition of aluminium to the structure does not lead to an increase in the number and strength of the acid centers. Although the true nature of this effect remains unclear, the influence of boron on aluminium incorporation in ZSM-5 has been reported, in terms of preferential location of B and Al in the zeolite network [28]. The results of the microcalorimetric experiments presented here clearly indicate that boron and aluminum have occupied such positions in the structure of the samples that these zeolites show only medium and weak acidity. This is due to the low amount of tetrahedral Al incorporated in the sample compared to extra-framework Al leading to the lack of very strong acid sites, as usually found in ZSM-5 zeolites. As presented in Figure 9, no sites with Q_{diff} > 120 kJ/mol were detected. The strengths in S-B1Al0, S-B2Al0 and S-B2Al2 can be classified as being of medium strength (120 kJ/mol < Q_{diff} < 80 kJ/mol) or weak (80 kJ/mol < Q_{diff} < 40 kJ/mol). Taking all of those findings in account it can be concluded that the incorporation of boron into zeolite framework is a complex process due to various simultaneous events occurring during the preparation process leading to the materials with specific properties.

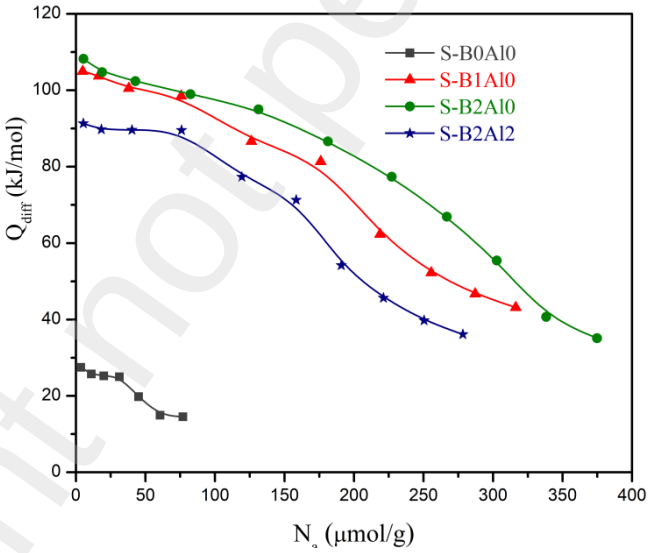

Figure 8. Calorimetric curves of ammonia adsorption on the studied series of samples.

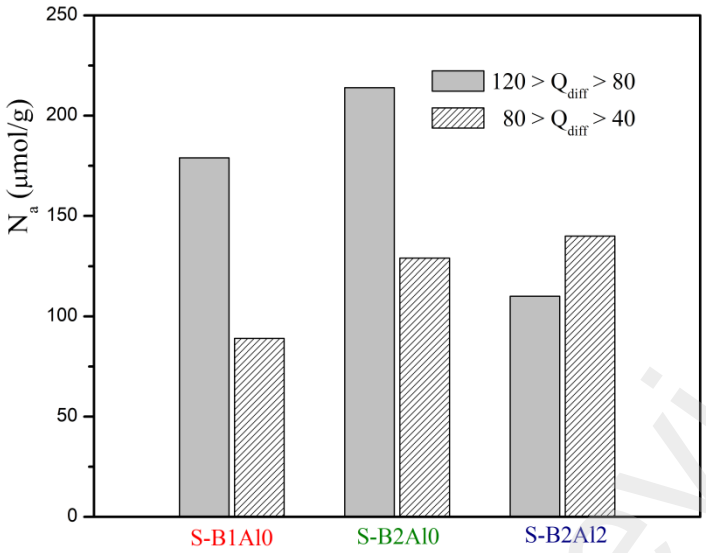

Figure 9. Distributions of strength of acidic sites.

Conclusions

In this work, we conducted synthesis and physico-chemical characterization of boron and boron-aluminium substituted MFI zeolites using different amounts of boron and aluminium. The performed analyses of the parent and modified zeolites obtained by hydrothermal treatment gave important insights into their structural, textural, morphological and acidic properties. XRD data show that all prepared zeolites are crystalline, regardless on the amount of heteroatom present in the starting reaction mixture. SEM micrographs show differences in the size and morphology of the obtained crystals. Local environments of aluminium and boron atoms, revealed by NMR spectroscopy, exhibit tetrahedrally coordinated framework, framework associated, and extra-framework boron species in boron-containing zeolites. Endothermic peaks maxima of boron-substituted zeolites are shifted to higher temperatures in TG curves compared to silicalite-1 giving clues on the importance of interactions of templates with heteroatoms. Consequently, the acidic properties of the samples, evaluated in terms of amount and strength show weak and moderate acid sites.

ACKNOWLEDGMENTS

The authors acknowledge the financial support by the Croatian Science Foundation, under project UIP-2019-04-4977 and the financial support by the Ministry of Science, Technological Development and Innovation of Republic of Serbia (Contract numbers: 451-03-65/2024-03/200146 and 451-03-65/2024-03/200116). The authors would like to thank

prof. Rastko Vasilić, University of Belgrade - Faculty of Physics, for performing X-ray diffraction analysis.

References

1. J. B.Nagy, R. Aiello, G. Giordano, A. Katovic, F. Testa, Z. Kónya, I. Kiricsi, Isomorphous Substitution in Zeolites, Mol Sieves 5 (2007) 365–478. https//doi.org/10.1007/3829_006

2. R. Millini, G. Perego and G. Bellusi, Synthesis and characterization of boron-containing molecular sieves, Topics in Catalysis 9 (1999) 13-34. https://doi.org/10.1023/A:1019198119365

3. S. Han, K.D. Schmitt, S.E. Schramm, P.T. Reischman, D.S. Shihabi, C.D. Chang, Isomorphous Substitution of Boron into Zeolites ZSM-5 and Y with Aqueous NH_4BF_4, J. Phys. Chem. 98 (1994) 4118-4124. https://doi.org/10.1021/j100066a035

4. C. Fild, D.F. Shantz, R.F. Lobo, H. Koller, Cation-induced transformation of boron-coordination in zeolites, Phys.Chem.Chem.Phys. 2 (2000) 3091-3098. https://doi.org/10.1039/B002134M

5. S-J. Hwang, C-Y Chen, S.I. Zones, Boron Sites in Borosilicate Zeolites at Various Stages of Hydration Studied by Solid State NMR Spectroscopy, J. Phys. Chem. B 108 (2004) 18535-18546. https://doi.org/10.1021/jp0476904

6. A. N. Petelski, N. M. Peruchena, M. F. Zalazar, Acidity of Isomorphic Substituted Zeolites with B, Al and Ga Revisited, 2024. Chem. Phys. Chem. e202400080. https://doi.org/10.1002/cphc.202400080

7. N. Cui, H. Guo, J. Zhou, L. Li, L. Guo, Z. Hua, Regulation of framework Al distribution of high-silica hierarchically structured ZSM-5 zeolites by boron-modification and its effect on materials catalytic performance in methanol-to-propylene reaction, Microporous Mesoporous Mater. 306 (2020) 110411. https://doi.org/10.1016/j.micromeso.2020.110411

8. C T-W. Chu, C.D. Chang, Isomorphous substitution in zeolite frameworks, 1. Acidity of surface hydroxyls in [B]-, [Fe]-, [Ga]- and [Al]-ZSM-5, J. Phys. Chem. 89 (1985) 1569-1571. https://doi/10.1021/j100255a005

9. S. P. Yuan, J. G. Wang, Y. W. Li, H. Jiao, Brønsted Acidity of Isomorphously Substituted ZSM-5 by B, Al, Ga, and Fe. Density Functional Investigations, J. Phys. Chem. A 106 (2002) 8167-8172. https://doi.org./ 10.1021/jp025792t

10. H. Tian, W. Li, L. He, Y. Zhong, S. Xu, H. Xiao, B. Xu, 2023. Rationalizing kinetic behaviors of isolated boron sites catalyzed oxidative dehydrogenation of propane, Nature Communications 14, 6520. https://doi.org/10.1038/s41467-023-42403-2

11. H. Zhou, X. Yi, Y. Hui, L. Wang, W. Chen, Y. Qin, M. Wang, J. Ma, X. Chu, Y. Wang, X. Hong, Z. Chen, X. Meng, H. Wang, Q. Zhu, L. Song, A. Zheng, F.-S. Xiao, Isolated boron in zeolite for oxidative dehydrogenation of propane, Science 372 (2021) 76–80. https://doi.org/ 10.1126/science.abe7935
12. N.R. Altvater, R.W. Dorn, M.C. Cendejas, W.P. McDermott, B. Thomas, A. J. Rossini, I. Hermans. B-MWW Zeolite: The Case Against Single-Site Catalysis. Angew. Chem. Int. Ed. 59 (2020) 6546 –6550. https://doi.org/10.1002/anie.201914696
13. P. Tian, Y. Wei, M. Ye, Z. Liu, Methanol to Olefins (MTO): From Fundamentals to Commercialization, ACS Catal. 5 (2015) 1922−1938. https//doi.org/10.1021/acscatal.5b00007
14. A. Xu , H. Ma , H. Zhang , W. Ying, D. Fang, Effect of boron on ZSM-5 catalyst for methanol to propylene conversion, Pol. J. Chem. Tech. 15 (2013) 95-101. https://doi.org/10.2478/pjct-2013-0075
15. H. Koller, C. Fild, R.F. Lobo, Variable anchoring of boron in zeolite beta, Microporous Mesoporous Mater. 79 (2005) 215–224. https://doi.org/10.1016/j.micromeso.2004.10.035
16. R. de Ruiter, A.P.M. Kentgens, J. Grootendorst, J.C. Jansen, H. van Bekkum, Calcination and Deboronation of [B]-MFI single crystals, Zeolites 13 (1993) 128-138. https://doi.org/10.1016/0144-2449(93)90072-B
17. H.T.T. Tong, H. Koller, Control of Al for B framework substitution in zeolite Beta by counterions, Microporous Mesoporous Mater. 148 (2012) 80-87. https://doi.org/10.1016/j.micromeso.2011.07.021
18. R. de Ruiter, J.C. Jansen, H. van Bekkum, On the incorporation mechanism of B and AI in MFI-type zeolite frameworks, Zeolites 12 (1992) 56-62. https://doi.org/10.1016/0144-2449(92)90011-D
19. R. de Ruiter, K. Pamin, A.P.M. Kentgens, J.C. Jansen, H. van Bekkum, Synthesis of molecular sieve [B]-BEA and modification of the boron site, Zeolites 13 (1993) 611-621. https://doi.org/10.1016/0144-2449(93)90132-M
20. D. Trong On, P. N. Joshi, S. Linguine, Synthesis, Stability and State of Boron in Boron-Substituted MCM-41 Mesoporous Molecular Sieves, J. Phys. Chem. 100 (1996) 6743-6748. https://doi.org/10.1021/jp953516r
21. C. Fild, H. Eckert, H. Koller, Evidence for Selective Association of Tetrahedral BO_4 Units with Na and of Trigonal BO_3 Units with H in Dehydrated Zeolite B-ZSM-5 from Solid-State NMR Spectroscopy. Angew. Chem. Int. Ed. 37 (1998) 2505-2507.

https://doi.org/10.1002/(SICI)1521-3773(19981002)37:18<2505::AID-ANIE2505>3.0.CO;2-F
22. T.I. Korányi, J.B. Nagy, Distribution of Aluminum and Boron in the Periodical Building Units of Boron-Containing β Zeolites, J. Phys. Chem. B 110 (2006) 14728-14735. https://doi.org/10.1021/jp0623185
23. T. Fu, L. Jia, G. Hou, Z. Li, 2023. Constructing silanol nests on ZSM-5 catalyst by deboronation for stable alkylation of toluene with methanol, Microporous Mesoporous Mater. 354, 112551. https://doi.org/10.1016/j.micromeso.2023.112551
24. E. Dib, J. Grand, S. Mintova, C. Fernandez, Structure-Directing Agent Governs the Location of Silanol Defects in Zeolites, Chem. Mater. 27 (2015) 7577–7579. https://pubs.acs.org/doi/10.1021/acs.chemmater.5b03668
25. I. C. Medeiros-Costa, E. Dib, N. Nesterenko, J-P. Dath, J-P. Gilson, S. Mintova, Silanol defect engineering and healing in zeolites: opportunities to fine-tune their properties and performances, Chem. Soc. Rev., 50 (2021) 11156-11179. https://doi.org/10.1039/D1CS00395J
26. L. Forni, G. Fornasari, G. Giordano, C. Lucarelli, A. Katovic, F. Trifirò, C. Perri, J. B. Nagy, Vapor phase Beckmann rearrangement using high silica zeolite catalyst, Phys. Chem. Chem. Phys. 6 (2004) 1842-1847. https://doi.org/10.1039/B316810G
27. M. Yabushita, R. Osuga, A. Muramatsu, Control of location and distribution of heteroatoms substituted isomorphously in framework of zeolites and zeotype materials, Cryst. Eng. Comm. 23 (2021) 6226-6233. https://doi.org/10.1039/d1ce00912e
28. C. Li, A. Vidal-Moya, P. J. Miguel, J. Dedecek, M. Boronat, A. Corma, Selective Introduction of Acid Sites in Different Confined Positions in ZSM-5 and Its Catalytic Implications, ACS Catal. 8 (2018) 7688–7697. https://doi.org/10.1021/acscatal.8b02112
29. J. Rouquerol, P. Llewellyn, F. Rouquerol, Is the BET equation applicable to microporous adsorbents?, Stud. Surf. Sci. Catal. 160 (2007) 49-56. https://doi.org/10.1016/S0167-2991(07)80008-5
30. Ch. Baerlocher, D.Brouwer, B. Marler, L.B. McCusker, Database of Zeolite Structures, http://www.iza-structure.org/databases/
31. W. Zhou, S-Y. Zhang, X-Y. Hao, H. Guo, C. Zhang, Y-Q. Zhang, S. Liu, MFI-type boroaluminosilicate: A comparative study between the direct synthesis and the templating method, J. Solid State Chem. 179 (2006) 855–865. https://doi.org/10.1016/j.jssc.2005.12.013

32. G. Boxhoorn, A.G.T.G. Kortbeek, G.R. Hays, N.C.M. Alma, A high-resolution solid-state29 Si n.m.r. study of ZSM—5 type zeolites, Zeolites 4 (1984) 15-21. https://doi.org/10.1016/0144-2449(84)90066-6
33. E. L. Wu, S. L. Lawton, D.H. Olson, A.C. Rohrman, G.T. Kokotailo, ZSM-5-type materials. Factors affecting crystal symmetry, J. Phys. Chem. 83 (1979) 2777–2781. https://doi.org/10.1021/j100484a019
34. N. Garcia Vargas, S. Stevenson, D.F. Shantz, Simultaneous isomorphous incorporation of boron and germanium in MFI zeolites, Microporous Mesoporous Mater. 170 (2013) 131–140. https://doi.org/10.1016/j.micromeso.2012.11.015
35. F. Crea, A. Nastro, J.B. Nagy , R. Aiello, Synthesis of silicalite-1 from systems with different TPABr/SiO_2 ratios, Zeolites 8 (1988) 262-267. https://doi.org/10.1016/S0144-2449(88)80121-0
36. M. Khatamian, A. Yavari, A. Akbarzadeh, E. Alizadeh. Synthesis and characterization of MFI-type borosilicate zeolites and evaluation of their efficiency as drug delivery systems. Mater. Sci. Engin. C 78 (2017) 1212–1221. https://doi.org/10.1016/j.msec.2017.03.008
37. R. Millini, G. Perego, D. Berti, W.O. Parker Jr., A. Carati, G. Bellussi. Structural characterization of as-synthesized B- and Ti-containing MFI-type molecular sieves. Microporous Mesoporous Mater. 35–36 (2000) 387–403. https://doi.org/10.1016/S1387-1811(99)00236-X
38. Y. Park, H. Koller, C. M. Lew, S. I. Zones, M. E. Davis, Correlating Local Geometry to ^{11}B NMR Chemical Shifts of Tetrahedrally Coordinated Boron in Molecular Sieves, J. Phys. Chem. C 128 (2024) 10705–10713. https://doi.org/10.1021/acs.jpcc.4c02361
39. P. Hudec, A. Smiešková, Z. Židek, P. Schneider, O. Ŝolcová, Determination of microporous structure of zeolites by t-plot method—State-of-the-art, Stud. Surf. Sci. Catal. 142 (2002) 1587-1594. https://doi.org/10.1016/S0167-2991(02)80328-7
40. A. Al-Dughaither, H. de Lasa, HZSM-5 Zeolites with Different SiO_2/Al_2O_3 Ratios, Characterization and NH_3 Desorption Kinetics, Ind. Eng. Chem. Res. 53 (2014) 15303-15316. https://doi.org/10.1021/ie4039532
41. M. Thommes, K. Kaneko, A.V. Neimark, J.P. Olivier, F. Rodriguez-Reinoso, J. Rouquerol, K.S.W. Sing, Physisorption of gases, with special reference to the evaluation of surface area and pore size distribution (IUPAC Technical Report), Pure Appl. Chem. 87 (2015) 1051–1069. https://doi.org/10.1515/pac-2014-1117

42. A. Cichocki, J. Parasiewicz-Kaczmarska, M. Michalik, M. Buś, Synthesis and characterization of boralites with the MFI structure. Zeolites 10 (1990) 577-582. https://doi.org/10.1016/S0144-2449(05)80315-X
43. H. Koller, C-Y. Chen, S.I. Zones, Selectivities in Post-Synthetic Modification of Borosilicate Zeolites, Top. Catal. 58 (2015) 451–479. https://doi.org/10.1007/s11244-015-0382-0
44. H. Liu, H. Ernst, D. Freude, F. Scheffler, W. Schwieger, In situ ^{11}B MAS NMR study of the synthesis of a boron-containing MFI type zeolite, Microporous Mesoporous Mater. 54 (2002) 319–330. https://doi.org/10.1016/S1387-1811(02)00392-X
45. R.M. Mihályi, G. Pál-Borbély, H.K. Beyer, Á. Szegedi, T.I. Korányi, Characterization of aluminum and boron containing beta zeolites prepared by solid-state recrystallization of magadiite, Microporous Mesoporous Mater. 98 (2007) 132–142. https://doi.org/10.1016/j.micromeso.2006.09.001
46. E.M. Flanigen, H. Khatami, H.A. Szymanski, Infrared Structural Studies of Zeolite Frameworks. In Molecular Sieve Zeolites-I, Am. Chem. Soc. 101 (1974) 201-229. https://doi.org/10.1021/ba-1971-0101.ch016
47. D. Lesthaeghe, P. Vansteenkiste, T. Verstraelen, A. Ghysels, C.E.A. Kirschhock, J.A. Martens, V. Van Speybroek, M. Waroquier, MFI Fingerprint: How Pentasil-Induced IR Bands Shift during Zeolite Nanogrowth, J. Phys. Chem. C 112 (2008) 9186-9191. https://doi.org/10.1021/jp711550s
48. A. Corma, C. Corell, J. Pérez-Pariente, J.M. Guil, R. Guil-López, S. Nicolopoulos, J. Gonzalez Calbet, M. Vallet-Regi, Adsorption and catalytic properties of MCM-22: The influence of zeolite structure, Zeolites 16 (1996) 7-14. https://doi.org/10.1016/0144-2449(95)00084-4
49. C. S. Blackwell, Investigation of zeolite frameworks by vibrational properties. 2. The double-six-ring in group 4 zeolites, J. Phys. Chem. 83 (1979) 3257–3261. https://doi.org/10.1021/j100488a015
50. A. Airi, M. Signorile, F. Bonino, P. Quagliotto, S. Bordiga, J.A. Martens, V. Crocellà, Insights on a Hierarchical MFI Zeolite: A Combined Spectroscopic and Catalytic Approach for Exploring the Multilevel Porous System Down to the Active Sites, ACS Appl. Mater. Interfaces 13 (2021) 49114−49127. https://doi.org/ 10.1021/acsami.1c11614
51. S. Bordiga, C. Lamberti, F. Bonino, A. Travert, F. Thibault-Starzyk, Probing zeolites by vibrational spectroscopies. Chem. Soc. Rev. 44 (2015) 7262-7341. https://doi.org/10.1039/c5cs00396b

52. V. Bernardet, A. Decrette, J-M. Simon, O. Bertrand, G. Weber, E-P. Bellat, Infrared Spectroscopic Study of Ethylene Adsorbed on Silicalite: Experiments and Molecular Dynamics Simulation. Adsorption 11 (2005) 383–389. https://doi.org/10.1007/s10450-005-5955-y

53. L. Regli, S. Bordiga, C. Lamberti, K. P. Lillerud, S. I. Zones, A. Zecchina, Effect of Boron Substitution in Chabazite Framework: IR Studies on the Acidity Properties and Reactivity Towards Methanol, J. Phys. Chem. C 111 (2007) 2992-2999. https://doi.org/10.1021/jp064048w

54. G. Ricchiardi, A. Damin, S. Bordiga, C. Lamberti, G. Spanò, F. Rivetti, A. Zecchina, Vibrational Structure of Titanium Silicate Catalysts. A Spectroscopic and Theoretical Study, J. Am. Chem. Soc. 123 (2001) 11409–11419. https://doi.org/10.1021/ja010607v

55. K. El-Egili, Infrared studies of Na_2O–B_2O_3–SiO_2 and Al_2O_3–Na_2O–B_2O_3–SiO_2 glasses, Physica B: Condensed Matter, 325 (2003) 340-348. https://doi.org/10.1016/S0921-4526(02)01547-8

56. D. Scarano, A. Zecchina, S. Bordiga, F. Geobaldo, G. Spoto, G. Petrini, G. Leofanti, M. Padovan, G. Tozzola, Fourier-transform infrared and Raman spectra of pure and Al-, B-, Ti- and Fe-substituted silicalites: stretching-mode region, J. Chem. Soc., Faraday Trans. 89 (1993) 4123-4130. https://doi.org/10.1039/FT9938904123

57. W-Y. Dong, Y-J.Sun, H-Y. He, Y-C. Long, Synthesis and structural characterization of B-Al-ZSM-5 zeolite from boron–silicon porous glass in the vapor phase, Microporous Mesoporous Mater. 32 (1999) 93-100. https://doi.org/10.1016/S1387-1811(99)00094-3

58. M. Soulard, S. Bilger, H. Kessler, J.L. Guth, Thermoanalytical characterization of MFI-type zeolites prepared either in the presence of OH^- or of F^- ions, Zeolites 7 (1987) 463-470. https://doi.org/10.1016/0144-2449(87)90016-9

59. M. Soulard, S. Bilger, H. Kessler, J.L. Guth, Characterization of the products remaining in the solid after partial thermal decomposition of Pr_4NF-, Pr_3NHF-, and Pr_4NOH-MFI precursors. Zeolites 11 (1991) 107-115. https://doi.org/10.1016/0144-2449(91)80403-M

60. S. Bilger, M. Soulard, H. Kessler, J.L. Guth, Identification of the volatile products resulting from the thermal decomposition of tetra-, tri-, di-, and mono-n-propylammonium cations occluded in MFI-type zeolites. Zeolites 11(1991) 784-791. https://doi.org/10.1016/S0144-2449(05)80056-9

61. G. Debras, A. Gourgue, J.B. Nagy, G. De Clippeleir, Physico—chemical characterization of pentasil type materials: II. Thermal analysis of the precursors, Zeolites 5 (1985) 377-383. https://doi.org/10.1016/0144-2449(85)90130-7

62. J. El Hage-Al Asswad, N. Dewaele, J.B. Nagy, R.A. Hubert, Z. Gabelica, E.G. Derouane, F. Crea, R. Aiello, A. Nastro, Identification of different tetrapropylammonium cations occluded in ZSM-5 zeolite by combined thermal analysis (t.g.-d.t.a.) and ^{13}C-n.m.r. spectroscopy, Zeolites 8 (1988) 221-227. https://doi.org/10.1016/S0144-2449(88)80311-7
63. H. Koller, R.F. Lobo, S.L. Burkett, M.E. Davis, SiO^-…HOSi Hydrogen Bonds in As-Synthesized High-Silica Zeolites, J. Phys. Chem. 99 (1995) 12588-12596. https://doi.org/10.1021/j100033a036